ACOUSTICS 2012

A beamforming strategy dedicated to post lens ultrasound imaging and ocular biometry using a 20 MHz multi-element probe

T. Mateo[a], Y. Mofid[b], J.-M. Grégoire[b] and F. Ossant[b]

[a]Imagerie et cerveau, Hôpital Bretonneau 1 Bd Tonnelle 37044 Tours
[b]Université François Rabelais de Tours, UMRS Imagerie et Cerveau, 10, boulevard Tonnellé, BP 3223, 37032 Tours Cedex 01, France
tony.mateo@etu.univ-tours.fr

Abstract—In the aim of improving ocular biometry using high resolution ultrasound imaging, acoustical properties of a porcine eye lens are investigated at high frequencies (10 to 24 MHz). The obtained values were used to perform a beamforming (BF) method dedicated to post lens imaging and whole eye biometry through a linear ultrasound (US) scanning using a 128 elements linear array working at 20 MHz. The probe was driven by an US research scanner developed in-house called the ECODERM. The performances of the developed BF method were compared with those of a classical BF having the same linear scanning. The comparison quantified both axial and lateral resolutions, image contrast, and the spatial mislocalization of reflectors observed beyond the lens.

1 Introduction

Ultrasound biomicroscopy [1] has taken an important place in ocular imaging, mainly to image the anterior segment (20 – 60 MHz) and occasionally the posterior segment (10 – 20 MHz) when OCT is ineffective e.g. cataract, leucoma. Especially, displaying the posterior segment is of clinical importance to diagnose pathologies such as macular degeneration, detached retina or retina vein occlusion.

However, the posterior coat resolution is poor and B-mode imaging resulting from classical beamforming with linear scanning suffers from geometrical distortion beyond the lens which affects biometry measurement. Hamidzada & al. reported a mean bias of -400 µm in the axial measurement of vitreous chamber depth, using a common velocity of 1550 m/s [2].

This bias is mainly due to the influence of the crystalline lens. Actually, due to an ultrasound celerity (about 1650 m/s in porcine eyes) around 10% higher than in the surrounding medium (aqueous/vitreous humor about 1500 m/s) and a biconvex geometry, the lens acts as a defocusing and refracting media for classical focused US beams.

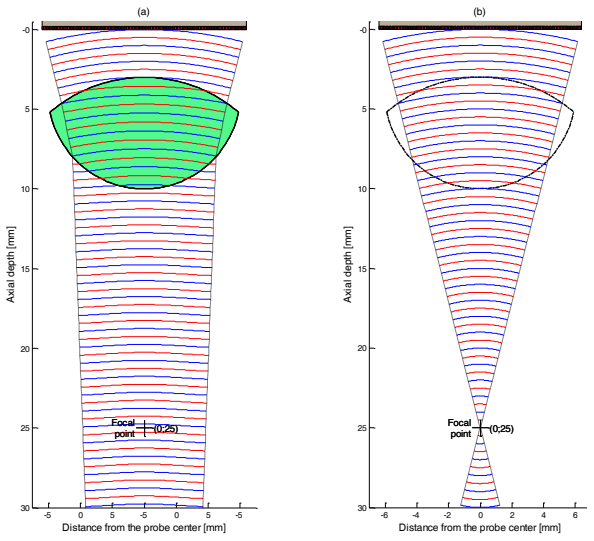

Figure 1: Propagation simulation of a wavefront focalized at 25 mm for an emission with 128 elements spaced by 100µm in the case of a homogeneous media where US celerity is 1500 m/s without lens interposed (b) and across the lens having 1650 m/s (a)

In figure 1 & 2, these effects are illustrated and highlighted in a realistic way thanks to a program running on Matlab specially developed to simulate the lens influence on a wavefront during its propagation. Refraction is taken into account according to Snell's law. Much kind of emissions and lens geometry can be evaluated. In fig. 1 the wavefront results from an aperture of 128 elements with 100µm spacing appropriately delayed to focus at 25 mm (diameter of a eyeball) in a media where US celerity is 1500m/s (humor mimicking). Lens celerity was set to 1650 m/s. Its geometry was closed to those of a porcine eye when no accommodation process occurs. Fig. 2-a represents the same lens and array but with a 32 elements scanning focalized at 15 mm in humor. In fig.2-b the scanning aperture is composed of 24 elements and lens geometry has been changed into its accommodation posture. Fig.1 illustrates mainly the lens defocusing effect and fig. 2 the significant refraction occurring especially on the edge of the lens during a US scan.

Currently, there is no beamforming strategy dedicated to ocular imaging despite the eye is an excellent subject for the development of imaging systems thanks to its regular geometry, the lack of overlying tissues, the homogeneity of the humorous tissue and the relatively low attenuation coefficient of the ocular tissue except for the lens.

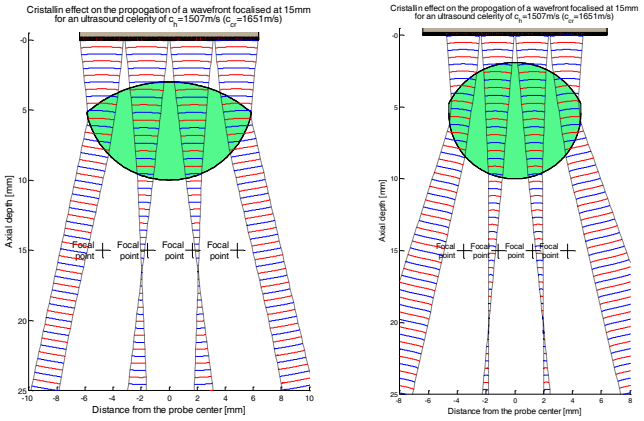

Figure 2: Propagation simulation of a wavefront focalized at 15 mm in a homogeneous media where US celerity is 1500 m/s during a scan with a 32 elements aperture (100µm spacing) across the lens (1650 m/s) without accommodation (left) and with 24 elements when accommodated (right)

In this paper, a dedicated beamforming method is therefore proposed to optimize the posterior coat US imaging beyond the lens and to improve the quality of US biometry measurements.

US imaging tests using the dedicated BF method were carried out on lenses coming from the porcine eye which is considered as a good animal model for the human eye in ultrasonic experiments according to many authors [3].

2 Material and methods

A porcine eye pair was obtained from National Research Institute in Agronomy (INRA – France) within 1 hour after sacrifice of the animals. We chose the eye from a healthy young animal (21 days).

The lens was reached from the back by cutting the eye around 1 mm under the limbus in order to pass under the ciliary body and then loosened by cutting the zonula fibres.

From the pair investigated one excised lens was dedicated to acoustical characterization measurement in double transmission (DT) and the other one to post lens US imaging.

Measurements were all done within 5 hours postmortem.

2.1 Acoustic properties of the porcine lens

DT measurements were carried out using a 27 MHz focused (5mm) mono-element transducer (PI 50 – 200171, Panametrics).

A pulser/receiver (5900 PR, Panametrics, Sofranel) having a 200 MHz bandwidth was driven the transducer in both transmitting and receiving with a 200 MHz pulse repetition frequency.

Acquired acoustic signals were digitized at 2.5 GHz with a digital phosphore oscilloscope (DPO4034B, Tektronix) on eight-bit resolution.

2.1.1 Lens acoustic celerity estimation

The lens was placed on a metal plate reflector in a degassed physiological saline solution (0.9%) as described in fig. 3. The transducer was then positioned right on the top of the lens along its anteroposterior axis where both lens sides could be assumed parallel regarding the beam width. That's why we performed celerity measurement only in the anteroposterior axis where beam is not reflected with an angle due to radii of curvature.

The technique used to measure the acoustic velocity was a classical differential pulse echo method. The reflector time of flight echo (t_r) was measured in the saline solution. Then, the ultrasound pulse was transmitted into the lens. The pulse was firstly reflected by the water/lens interface (t_l) and secondly by the lens/reflector interface (t_r').

From the estimated value of c_{lens} and the time interval $\Delta t = t_r' - t_l$ the anteroposterior thickness was deduced according to following relation:

$$d_{lens} = c_{lens} \frac{t_r' - t_l}{2} \quad (1)$$

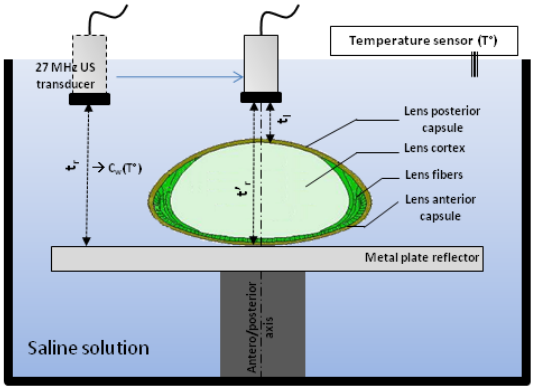

Figure 3: Schema of the celerity and attenuation measurement

The lens velocity was then calculated from the known velocity in physiological saline solution using the temperature measured by a platine probe (P 655-LOG, Dostmann):

$$c_{lens}(T°) = c_{water}(T°) \times \left[\frac{t_r - t_l}{t_r' - t_l} \right] \quad (2)$$

2.1.2 Lens attenuation estimation

The lens frequency dependent attenuation coefficient was calculated from the t_r' and t_r echoes spectrum of the two metal plate reflection (in saline solution and beyond the lens) and d_{lens} as follows :

$$\alpha_{lens}(f) = -\frac{10}{2d_{lens}} \log_{10}\left(\frac{S_{lens}(f)}{T_{lens/water}^{\ 2} \times S_{water}(f)} \right) \quad (3)$$

Where

S_{water} is the power spectra of the plate reflection in water

S_{lens} is the power spectra of the plate reflection with lens interposed

And $T_{lens/water}$ the back and forth transmission coefficient between lens and water calculated following Eq. (4).

Otherwise, a high accuracy balance (A&D – HR 200, ±0.1mg) was used in order to determine the lens masse and its volume according to Archimed's principle in order to find the lens density (ρ_{lens}) necessary to appreciate its acoustical impedance (Z_{lens}).

$$T_{lens/water} = T_{lens \to water} \times T_{water \to lens} = \frac{4 Z_{water} Z_{lens}}{\left(Z_{water} + Z_{lens} \right)^2} \quad (4)$$

The acoustic impedance in the lens measurement served to take in consideration transmission coefficient in both back and forth. The reflection coefficient on the metal reflector was considered equal to 1. This leads us to not underestimate the attenuation coefficient.

The US attenuation in the saline solution at 20MHz is assumed negligible.

2.2 High frequency US imaging with multi-elements probe

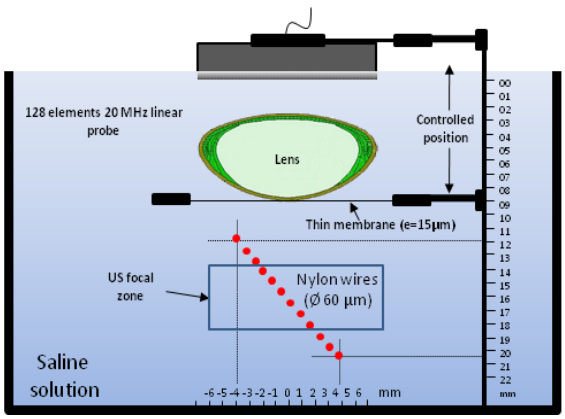

Figure 4: Schema of the US imaging measurement

Ultrasound linear imaging was performed using the ECODERM research scanner developed in- house. This system has 128 individually programmable transmitters capable of applying focalization delays thanks to its 500 picoseconds precision. The transmitters emit a unipolar pulse with -100 V amplitude and 10 ns duration, giving a 150 MHz -6 dB bandwidth. The 128 receivers have an individual pre-amplifier with adjustable gain varying from 30 to 75 dB within a 120 MHz – 3dB bandwidth. Sixteen receive channels are sampled simultaneously from 50 to 400 MHz with a precision of 12 bits.

The ECODERM has two ways of functioning. One way for real time imaging (FPS=40 Hz) clinically used with beamformation embedded and the other way for research purpose allowing to control independently for each emission the number of emitters with their respective delays (from 0 to 125.5 nanoseconds) and the number of receivers from 1 until 128 by multiplexing. The research mode provides raw ultrasound radio-frequency data which are then post-processed with the desired receive beamforming method.

The ECODERM was employed with a 20 MHz ultrasonic linear probe (Vermon, Co., France) having 100 µm pitch, 10 µm kerf and 3 mm elevation width focalized around 14 mm in water at 25 °C. The probe positioning was adjusted by a 3-D translation system (DC 500 - stepsize 0.5µm).

Furthermore, we used the second lens (from the same pair) to B-mode imaging, working with the acoustical celerity previously measured on the first lens. Lens was placed around 3 mm under the probe on a thick plastic membrane (15 µm) maintained by a rigid support (fig. 4). A homemade ultrasound high resolution phantom consisting of nylon wires (Ø 60µm) diagonally spaced with 0.7 to 1 mm spacing (axial and lateral) was placed beyond the lens.

The wire diameter was considered small enough regarding the wavelength in water at 20 MHz (75µm) to allow axial and lateral resolution quantification.

We performed a linear scanning with 24 elements in emission focalized at 15mm (center of the wires phantom) and 64 elements in reception. Two US images were then reconstructed. The first US image was obtained from a classical reconstruction i.e. the acquired raw data were classically beamformed with a dynamical focalization in reception where observed media is considered homogeneous. The second US image was obtained from a dedicated reconstruction process considering the lens acoustical properties especially its celerity. The two echographics images, post-processed through the same raw data, are presented hereafter as images with classical BF and with dedicated BF respectively.

A reference acquisition of the wires phantom was made in pure water (fig. 7-a) in exactly the same probe position as with the lens interposed. The obtained image was used as a reference to quantify spatial mislocalizations of the wires between classical BF and dedicated BF when lens interposed.

3 Results

3.1 Acoustic properties of the porcine lens

Lens celerity was estimated thanks to the following echograms (fig. 5). Spectrums of the reflectors echoes in saline solution and through the lens were used to deduce the lens attenuation (fig. 6). The measured parameters are summarized in Table I where α_1 and β are respectively the attenuation slope and the attenuation intercept calculated by a linear fit.

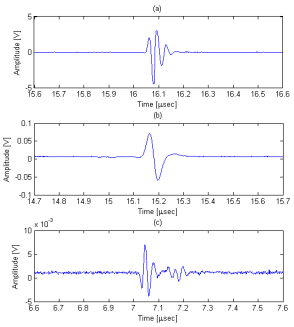

Figure 5: (a) Radiofrequency echogram of the reflector in saline solution (0.9%); (b) RF echogram of the reflector after lens crossing, (c) RF echogram of the saline solution /lens interface

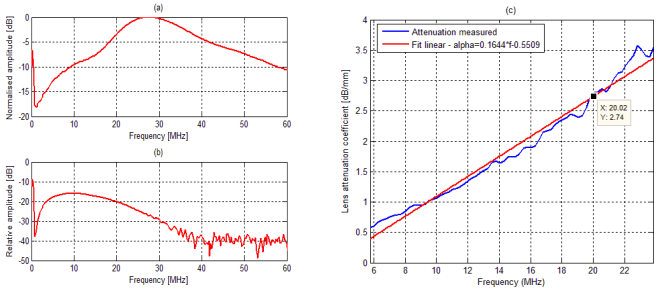

Figure 6: (a) Amplitude spectra of the reflector in saline solution (0.9%), (b) Amplitude spectra of the reflector after lens crossing, (c) Attenuation coefficient of the porcine lens with linear regression fit

Lens parameters measured from a 21 days aged pig at 22.4 °C						
c_{lens} [m/s]	d_{lens} [mm]	α at 20 MHz [dB/mm]	α_1 [dB/mm/MHz]	β [dB/mm]	ρ_{lens} [kg/m^3]	Z_{lens} [MRayl]
1651	7.85	2.74	0.1644	-0.5509	1118.5	1.846

Table 1: Acoustical parameters measured

3.2 20 MHz imaging through the lens with multi-element probe

Each image here presented has been log-compressed and normalized according to :

$$S_{\log} = 20\log_{10}\left(\frac{S_{env} - \min(S_{env})}{\max(S_{env}) - \min(S_{env})}\left(G_S - 1\right) + 1\right) \quad (5)$$

where S_{env} is the envelop of the BF data and G_S is linked to the dynamic range by $G_S = 10^{\frac{DR}{20}}$.

All the quantitative results summarized in table II came from the analysis of the points spread functions (PSF) contained in the region of interest (ROI) highlighted in each image of fig. 7. The index "Ref.", "w" and "~~w~~" correspond respectively to the PSF from the reference image (fig. 7-a), the classical BF image (fig. 7-b) and the dedicated BF image (fig. 7-c). The PSF are numbered with depth increasing.

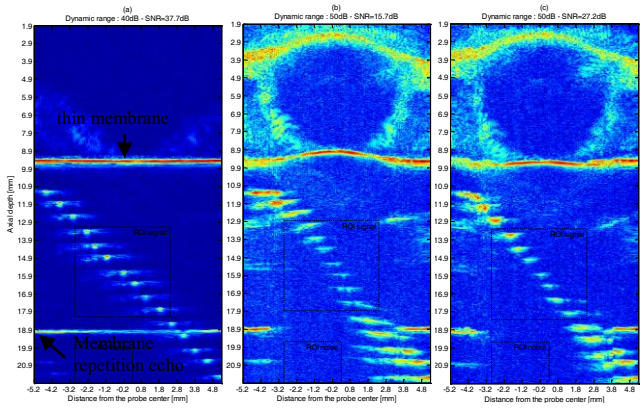

Figure 7: B-mode of the wire phantom without lens interposed used as reference (a), through the lens with classical BF (b) and with dedicated BF (c)

The table is divided in two parts. One for spatial fidelity evaluation where axial and lateral errors are calculated from the PSF centers. The reference coordinates are determined from the corresponding PSF of fig. 7-a. The PSF center coordinates were evaluated by calculating the spatial centroid of all PSF pixels within -6 dB from its maximum value. Spatial mislocalization corresponds to the modulus of axial and lateral errors.

The other part presents the image quality factors. Axial and lateral resolution were calculated at -6dB. For each PSF, relative gain between dedicated BF and classical BF and then reference were respectively calculated according to:

$$G_{w/\bar{w}}(i)=20\log_{10}\left(\frac{\max\left(PSF_{w}(i)\right)}{\max\left(PSF_{\bar{w}}(i)\right)}\right) \quad G_{w/ref}(i)=20\log_{10}\left(\frac{\max\left(PSF_{w}(i)\right)}{\max\left(PSF_{ref}(i)\right)}\right) \quad (6)$$

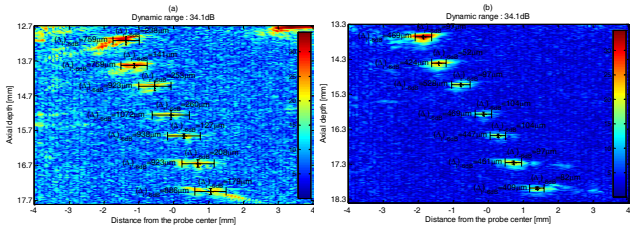

Figure 8: Axial and lateral resolution of the PSF resulting from classical BF (a) and dedicated BF (b) displayed both with 34.1dB Dynamic

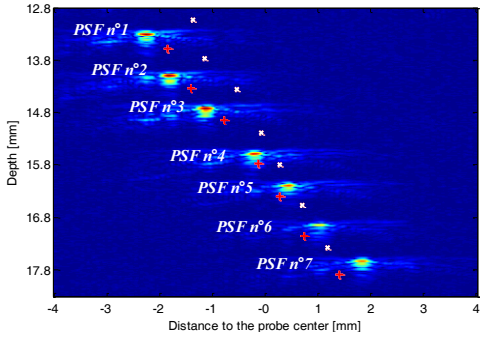

Figure 9: Superposition on the reference image of the PSF centers from classical BF (white crosses) and dedicated BF (red crosses)

In fig.8, axial and lateral resolution are represented in the ROI zoomed from fig. 7-b & c. Dynamic range is the same for both images.

Finally spatial mislocalization is highlighted in fig. 9 thanks to the superposition of the PSF centers in the ROI coming from classical and dedicated BF on the reference image.

4 Discussion

Crystalline lens attenuation and celerity measurements performed in the first part of the study were in good agreement with the data literature [3].

Image distortion when performing a classical BF through the lens was clearly demonstrated when regarding how the wire phantom and the plane thin membrane are far from their known geometry and location (fig. 7-b).

This spatial distortion was greatly reduced when applying a beamforming strategy taking into account the lens effects evaluated by acoustical measurements.

Compared to classical beamforming, the signal to noise ratio (SNR) was improved by an average of 8.1 ± 2.5 dB after the lens crossing. The values taken by $G_{w/ref}$ agree for each PSF with the lens attenuation measurement and the lens thickness crossed towards the PSF. The weakest relative gain with -21.6dB was logically reached by PSF n°4 where the lens thickness to cross back and forth was the largest.

Spatial resolution was enhanced by a factor 2 both axially and laterally. Spatial errors regarding the original geometry of the observed media were reduced by 47% axially and 38 % laterally. Thus, the global spatial localization accuracy has been improved by 44%.

Globally, the spatial distortion introduced by the lens on ultrasound imaging was significantly reduced by the dedicated BF presently developed compared to a conventional classical BF using the same emission and receptors elements. The original geometry of the post lens reflectors including the thin membrane was clearly more preserved when BF correction was applied.

With such a method typical biometrics measurements e.g. eye diameter, posterior chamber length or lens thickness, can be appreciated with a better accuracy than in conventional ocular US imaging.

The spatial localization beyond the lens could still be improved by a better appreciation of its inhomogeneity thus allowing accurate US ocular biometry.

Acknowledgment

The ECODERM system development was supported by Cosmetic Valley, OSEO, Tour(s) Plus, CG37 and Region Centre.

Author thanks Laurent COLIN (CETU Althaïs) for his very helpful support on the ECODERM debugging. Thanks to Jean-Yves TARTU for his precious creations. Special thanks for the delicate presence of Gwenaëlle and Marie-Jo.

References

[1] F. S. Foster, C. J. Pavlin, K. A. Harasiewicz, D. A. Christopher, and D. H. Turnbull, “Advances in ultrasound biomicroscopy,” Ultrasound in Med & Biol, vol. 26, No. 1, pp. 1–27, 2000.

[2] W.A. Hamidzada, and E. P. Osuobeni, “Agreement between A-mode and B-mode ultrasonography in the measurement of ocular distances”, Vet Radiol & Ultrasonography, vol. 40, pp. 502-507, No. 4, 1999.

[3] C. L. de Korte, A. F. W. van der Steen, adnd J.M. Thijssen, “Acoustic velocity and attenuation of eye tissues at 20 MHz”, Ultrasound in Med & Biol, vol. 20, No. 5, pp. 471–480, 1994.

Table 2: Quantitative analysis of the nylon wires PSF in the region of interest

	Parameter		Point Spread Function							Mean Value ± SD
			N°1	*N°2*	*N°3*	*N°4*	*N°5*	*N°6*	*N°7*	
SPATIAL FIDELITY	Spatial mislocalization $\sqrt{Err_r^2 + Err_l^2}$ [µm]	~~w~~	966	795	743	517	515	566	722	**689 ± 163**
		w	484	468	414	209	262	363	495	**385 ± 128**
	Axial error Err_r [µm]	~~w~~	-395	-437	-464	-502	-493	-473	-346	**444 ± 52**
		w	271	235	225	199	217	228	269	**235 ± 24**
	Lateral error Err_l [µm]	~~w~~	882	664	580	124	-148	-310	-634	**477 ± 266**
		w	401	405	347	63	-146	-283	-416	**294 ± 129**
IMAGE QUALITY	Axial resolution $(\Delta r)_{-6dB}$ [µm]	Ref.	37	37	45	37	45	37	82	**46 ± 21**
		~~w~~	238	141	253	260	127	208	193	**203 ± 49**
		w	97	52	97	104	104	97	82	**90 ± 17**
	Lateral resolution $(\Delta l)_{-6dB}$ [µm]	Ref.	231	201	208	216	223	268	246	**227 ± 15**
		~~w~~	759	759	923	1072	938	923	1124	**928 ±129**
		w	469	424	528	469	447	461	409	**458 ± 35**
	Relative gain [dB]	$G_{w/\bar{w}}$	12,3	9,1	5,7	6,3	5,34	9,4	8,8	**8,1 ± 2,5**
		$G_{w/ref}$	-7	-14,1	-21,2	-21,6	-19	-8,7	-13, 1	**-15 ± 5,9**